BCSJ

Document type: Review/Account

Award Account

The Chemical Society of Japan Award for Creative Work for 2014

MAIRS: Innovation of Molecular Orientation Analysis in a Thin Film

Takeshi Hasegawa* and Nobutaka Shioya

Institute for Chemical Research, Kyoto University, Gokasho, Uji, Kyoto 611-0011, Japan

E-mail: htakeshi@scl.kyoto-u.ac.jp

Received: April 30, 2020; Accepted: May 14, 2020; Web Released: May 22, 2020

Takeshi Hasegawa

Takeshi Hasegawa received his PhD from Kyoto University. He was appointed Assistant Professor at Kobe Pharmaceutical University in 1993 and Lecturer in 2001. After serving as Associate Professor at CIT, Nihon University (2003), Researcher at JST PRESTO (2004), and Associate Professor at Tokyo Institute of Technology (2006), he joined ICR, Kyoto University as Full Professor in 2011. He is a Fellow of the Society for Applied Spectroscopy (USA) after recognition of his original spectroscopic technique of "pMAIRS." Fluorine chemistry on stratified dipole-arrays (SDA) theory is another topic of interest for him.

Abstract

Multiple-angle incidence resolution spectrometry (MAIRS), originally developed in our group, is a unique spectroscopic technique for analyzing the structure of molecular aggregates in a thin film, which requires only the refractive index of the film for attaining an analytical accuracy of three significant digits. Since MAIRS is robust to the surface roughness of the film, rough films prepared by using the spin-coating, bar-coating, or drop-casting techniques can be analyzed with a good reproducibility. MAIRS makes the best use of a Fourier transform infrared (FT-IR) spectrometry, which enables us to discuss molecular conformation, packing, polymorphs etc. as well as the molecular orientation. At the moment, MAIRS has two options, pMAIRS and MAIRS2. pMAIRS has already been established and the application is spreading. MAIRS2 is the newest technology, which frees us from FT-IR specific problems, that is to say, interference of water-vapor peaks and of optical fringes. In this review, the cutting-edge analytical technology of MAIRS is described comprehensively for convenience of both pMAIRS and MAIRS2 users.

Keywords: MAIRS | Molecular orientation | Organic semiconductors

1. Introduction

On developing materials with new functions and properties, material design tends to be oriented to "molecular" design. The primary chemical structure of a compound influences the material properties indeed, but a direct correlation between the structure and property is not expected, even if the higher-order structure and the regioregularity of the compound are both controllable. What we need for bridging the molecular structure and the material properties is the aggregation structure of the molecules, which depends on molecular orientation, packing and polymorphs at least. Accurate prediction of the aggregation structure solely on the primary chemical structure is, however, close to impossible, and therefore analysis of aggregation structure of the developed material is a crucial key to feedback to the molecular design.

Molecular devices, for example, are mostly built in a thin film for a high throughput of electron transport, since the exciton radius is small for organic compounds requiring a thin layer. A typical device is a photovoltaic that has a layered structure sandwiched by metal and transparent electrodes. Since the direction of the molecular stacking of aromatic rings is suitable for the electron transport, the molecular plane should be stacked with a face-on orientation to the film surface. In this manner, we have to control the molecular arrangement in a thin film by monitoring the molecular orientation of each chemical group.

To monitor the molecular arrangement in a thin film, two analytical approaches are fundamental and necessary: crystallography and spectroscopy that reveal polymorph and molecular orientation, respectively. For the polymorph analysis, two-dimensional grazing incidence X-ray diffraction (2D-GIXD) is recognized to be most powerful to look over a wide range of the reciprocal lattice at once. Regardless, very limited information is given for an amorphous part by the diffraction technique. Spectroscopy is, on the other hand, suitable for discussing the molecular orientation of each chemical group irrespective of crystallinity.

Multiple-angle incidence resolution spectrometry (MAIRS) meets the spectroscopic analytical purpose in a thin film. MAIRS makes the best use of Fourier transform infrared spectrometry (FT-IR), in terms of the quantitative accuracy and the sensitivity for the monolayer-level thin films. MAIRS is characterized to enable us to perform quantitative analysis of molecular orientation with no optical parameter for many compounds. In addition, MAIRS has a great advantage that a thin film with a rough surface can accurately be analyzed with a good reproducibility. If the film comprises crystallites, the MAIRS spectra and GIXD patterns can cooperatively be discussed to reveal an actual image of the molecular aggregation structure in the film. In this sense, the combination of MAIRS and GIXD is most useful and powerful for the development of functionalized thin films.

In this review, a development history of the MAIRS technique is described from the research background to state of the art of the technique involving practical applications.

2. Fundamental of Molecular Orientation Analysis Using Conventional Absorption Spectroscopy

Spectroscopic analysis of molecular orientation in a thin film is powerful especially when vibrational spectroscopy is employed, since the orientation of each chemical group can be analyzed no matter what the crystallinity is in the film. When infrared (IR) spectroscopy is employed, in particular, the analysis is much easier than the other techniques because of two reasons. The first one is that the peak intensity (absorbance), A, is simply proportional to the squared inner product of the transition moment, $\langle k|r|j\rangle$, and the electric field, E, of the IR light as indicated by Fermi's golden rule (eq 1).[1]

$$A \propto |q\langle k|r|j\rangle \cdot E|^2 \quad (1)$$

Here, q is the charge on the dipole moment. The direction of the electric field can easily be controlled by rotating a linear polarizer, which make it possible to determine the direction of the transition moment experimentally.

Secondly, the direction of the transition moment is easily determined because of another simple relationship: the irreducible representations of $\langle k|$ and r are identical to each other, so that the transition moment must be non-zero in group theory.[1,2]

In short, the molecular orientation can experimentally be analyzed through determination of the direction of the transition moment, which is simply done by rotating a linear polarizer.

The most fundamentally important techniques for discussing the molecular orientation in a thin film[1,3,4] are the normal-incidence transmission (Tr) and reflection-absorption (RA)[5] techniques. The optical schemes are presented in Figure 1. For the RA measurements, a grazing angle is used for the incidence typically at 80° from the surface normal, and the p-polarization is used. The electric field of the IR light is parallel to the substrate surface for the Tr measurements, whereas it is perpendicular to the surface for the RA measurements. As a result, therefore, the surface-parallel and -perpendicular components of a transition moment are selectively observed in the Tr and RA spectra, respectively, which are the complementary *surface selection rules*.[1,2,4]

Example spectra of the two spectrometries are presented in Figure 2. The two figure panels show high and low wavenumber regions of IR Tr and RA spectra of a 7-monolayer Langmuir-Blodgett (LB) film of cadmium stearate. For the Tr measurement, an IR transparent substrate of calcium fluoride (CaF_2) is used; whereas a silver-evaporated glass slide is used for the RA measurement.

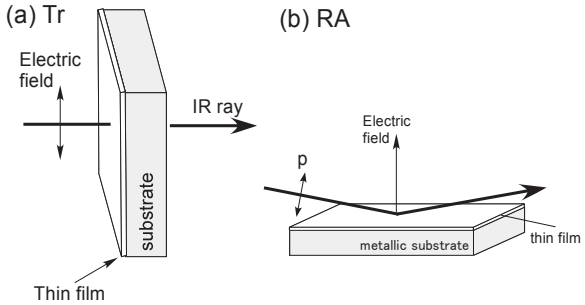

Figure 1. Schematics of (a) Tr and (b) RA measurements of a thin film on IR transparent and metallic substrates, respectively. For the RA measurements, the p-polarized ray is employed.

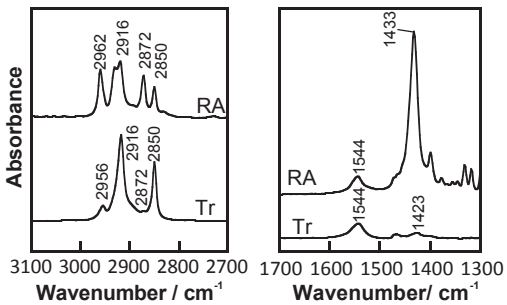

Figure 2. IR Tr and RA spectra of a 7-monolayer LB film of cadmium stearate deposited on CaF_2 and silver substrates, respectively. The two spectra are plotted with a common ordinate scale.

As found in Figure 2, the RA and Tr spectra in the higher-wavenumber region (left panel) seem to have a similar peak intensity to each other; whereas they have different intensity in the lower-wavenumber region (right panel). These unbalanced intensities are caused by the difference of the ordinate scales of the two spectrometries. As a matter of fact, the RA spectrometry has an apparently larger intensity than that of the Tr by a factor of nearly one order of magnitude.[1,2] In the case of Figure 2, therefore, the RA spectrum should be corrected to be weaker by a factor of ca. 0.1 for comparison to the Tr one. To correct the ordinate scales quantitatively, many optical parameters involving complex refractive index as a function of wavenumber and thickness are definitely needed for the calculation,[6] which makes the conventional IR spectroscopy unpractical for many users.

We also have to note that having "anisotropic optical parameters" a priori is equal to having the orientation angles before the analysis, which is indeed a big dilemma. Analysis of molecular orientation using two different techniques has thus a high hurdle for practical use.

If the ordinate scales could be arranged to be common to the two techniques, therefore, the molecular orientation angle, ϕ, should easily be analyzed in a very simple manner, if the real part of refractive index can be approximated to be a constant, which corresponds to a weak absorption.[1,4,6]

$$\phi = \tan^{-1}\sqrt{\frac{2A^{\mathrm{Tr}}}{A^{\mathrm{RA}}}} \tag{2}$$

Note that, in this equation, no optical parameter is involved for the orientation analysis on the uniformed ordinate scale.

This analytical dream comes true, if an idea of multivariate analysis is added to the conventionally established physically rigorous theory.

3. Birth of MAIRS

To overcome the limit of the physical principle, multivariate analysis is introduced to make the best use of the theoretical fundamentals of spectroscopy as a new spectroscopic strategy.

In the new strategy, the conventional Tr and RA measurements are changed to new schematics using a common normal-incidence Tr geometry[7] as shown in Figure 3.

The schematic of the in-plane (IP) measurement (Figure 3a) is the same as that of the conventional Tr measurements (Figure 1a). On the other hand, the out-of-plane (OP) measurement is realized by using a virtual light that has an electric-field oscillation parallel to the light-traveling direction (Figure 3b), which is not available in nature. If the light intensities of both IP and OP measurements were readily measured, nevertheless, a unique measurement scheme would be built as follows.

In practice, the IR ray is incident on the sample (a thin film deposited on a substrate) obliquely at the angle of incidence of θ, and the intensity of the transmitted light ($\boldsymbol{s}_{\mathrm{obs}}$) is measured as a single-beam measurement by FT-IR as shown in Figure 4.

Here, $\boldsymbol{s}_{\mathrm{obs}}$ involves a linear combination of $\boldsymbol{s}_{\mathrm{IP}}$ and $\boldsymbol{s}_{\mathrm{OP}}$ with weighting ratios of r_{IP} and r_{OP}, whereas the rest factors (e.g. reflected ray) with no linear correlation with the weighting factors are out of the linear combination. Fortunately, on changing the angle of incidence, the linear combination part can be tied up in a classical least-squares (CLS) regression[1] manner (eq 3) leaving the remaining parts in $\boldsymbol{U}$. Here, $\boldsymbol{U}$ is a "garbage matrix" that *receives the non-linear responses* to the weighting ratio matrix, $\boldsymbol{R}$, which is a unique characteristic of using a regression equation.[1]

$$\boldsymbol{S} \equiv \begin{pmatrix} \boldsymbol{s}_{\mathrm{obs},1} \\ \boldsymbol{s}_{\mathrm{obs},2} \\ \vdots \end{pmatrix} = \begin{pmatrix} r_{\mathrm{IP},1} & r_{\mathrm{OP},1} \\ r_{\mathrm{IP},2} & r_{\mathrm{OP},2} \\ \vdots & \vdots \end{pmatrix} \begin{pmatrix} \boldsymbol{s}_{\mathrm{IP}} \\ \boldsymbol{s}_{\mathrm{OP}} \end{pmatrix} + \boldsymbol{U} \equiv \boldsymbol{R}\begin{pmatrix} \boldsymbol{s}_{\mathrm{IP}} \\ \boldsymbol{s}_{\mathrm{OP}} \end{pmatrix} + \boldsymbol{U} \tag{3}$$

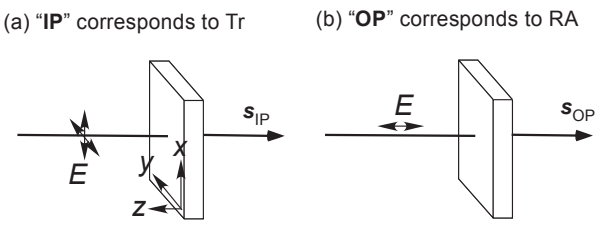

Figure 3. Schematics of (a) MAIRS-IP and (b) –OP measurements of a thin film (not drawn) deposited on an IR transparent solid substrate. The double arrow indicates the direction of the electric field oscillation of the IR ray. For the IP measurements, two degrees of freedom are both indicated by the two double arrows.

Here, the matrix element of $\boldsymbol{R}$ is theoretically obtained[7] as eq 4.

$$\boldsymbol{R} = \begin{pmatrix} 1 + \cos^2\theta_j + \sin^2\theta_j \tan^2\theta_j & \tan^2\theta_j \\ \vdots & \vdots \end{pmatrix} \tag{4}$$

This matrix proved to be physically correct, which needs heavy mathematical calculations though.[8]

Then, what we have to do is collect single-beam spectra at multiple angles of incidence for both sample and background measurements. Note that single-beam (light intensity) spectra are collected, and absorbance spectra cannot be used.[1,7] The set of angle-dependent single-beam spectra are stored in $\boldsymbol{S}$ in eq 5, and both $\boldsymbol{s}_{\mathrm{IP}}$ and $\boldsymbol{s}_{\mathrm{OP}}$ are quickly calculated by using eq 5 as the least-squares solution[1] of eq 3.

$$\begin{pmatrix} \boldsymbol{s}_{\mathrm{IP}} \\ \boldsymbol{s}_{\mathrm{OP}} \end{pmatrix} = (\boldsymbol{R}^{\mathrm{T}}\boldsymbol{R})^{-1}\boldsymbol{R}^{\mathrm{T}}\boldsymbol{S} \tag{5}$$

This set of measurements and calculation is carried out for both sample (S) and background (B) measurements, which finally yields the IP and OP spectra, $\boldsymbol{A}_{\mathrm{IP}}$ and $\boldsymbol{A}_{\mathrm{OP}}$, as follows.

$$\begin{aligned} \boldsymbol{A}_{\mathrm{IP}} &= -\log(\boldsymbol{s}^{\mathrm{S}}_{\mathrm{IP}}/\boldsymbol{s}^{\mathrm{B}}_{\mathrm{IP}}) \\ \boldsymbol{A}_{\mathrm{OP}} &= -\log(\boldsymbol{s}^{\mathrm{S}}_{\mathrm{OP}}/\boldsymbol{s}^{\mathrm{B}}_{\mathrm{OP}}) \end{aligned} \tag{6}$$

Here, the division is carried out at each wavenumber. This is the basic framework of the measurements of MAIRS spectra, but at the moment, the ordinate scales are not uniformed. For a quantitatively accurate analysis, precise optimization of the angle of incidence considering the refractive index is necessary, which is described in Section 6.

These spectra correspond to the conventional Tr and RA spectra in shape.[7] In particular, the IP spectrum agrees with the Tr spectrum quantitatively with a better signal-to-noise ratio.[9]

4. pMAIRS

The original MAIRS technique stated in Section 3 works well to reveal the spectral 'shape' of the IP and OP spectra, but the ordinate scale of the OP spectrum has sometimes a large inaccuracy. This is mostly due to the apparent polarization dependence of FT-IR. Indeed, the observed intensity ratio of the s-polarization to the p-polarization is apart from unity, which depends on wavenumber.

To eliminate the polarization dependence, the s-polarization is removed from the MAIRS measurements, and only the p-polarization should be employed for the analysis. This is called the p-polarization MAIRS or "pMAIRS."[10]

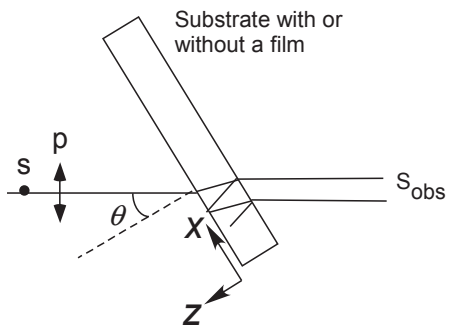

Figure 4. Measurement scheme of MAIRS. The thin film is omitted, and the side view of the substrate only is illustrated. s and p denote the polarizations.

pMAIRS has a slightly different weighting matrix, $\boldsymbol{R}_{\mathrm{p}}$, from that of the original MAIRS as is presented in eq 7.

$$\boldsymbol{R}_{\mathrm{p}} = \begin{pmatrix} \cos^2\theta_j + \sin^2\theta_j \tan^2\theta_j & \tan^2\theta_j \\ \vdots & \vdots \end{pmatrix} \tag{7}$$

$\boldsymbol{R}_{\mathrm{p}}$ is obtained by removing "1" in $\boldsymbol{R}$ (eq 4), which corresponds to the s-polarization, leaving the remaining matrix elements as they are. With the pMAIRS technique, the analytical accuracy becomes quite high, and reproducibility is also high.

Since the p-polarization provides electric fields in the x- and z-directions (Figure 4), pMAIRS is theoretically suitable for analyzing not only a uniaxially distributed molecule, but also for a biaxially distributed system. For analyzing the biaxial system, the sample film is once measured by pMAIRS, followed by a similar measurement with a rotated sample by 90° in the film plane.

5. Intuitive Understanding of pMAIRS

The pMAIRS-IP and -OP spectra are extracted from a collection of multiple single-beam spectra measured at various angles of incidence as the least-squares solution.

Since the reader may be confused on the extraction mechanism on eqs 3 and 4, the mathematical process is explained intuitively by using a schematic in Figure 5.

The matrix of $\boldsymbol{S}$ is a linear combination of $\boldsymbol{s}_{\mathrm{IP}}$ and $\boldsymbol{s}_{\mathrm{OP}}$ as found in eq 3. Linear combination of the two vectors means that all the points stored in $\boldsymbol{S}$ should be involved in two-dimensional space, i.e., a plane, which is spanned by the vectors of $\boldsymbol{s}_{\mathrm{IP}}$ and $\boldsymbol{s}_{\mathrm{OP}}$ (Figure 5).

A point in the plane corresponds to a measured spectrum, and the position is a function of the angle of incidence.[1] pMAIRS extrapolates some of the points by the least-squares line to have the optimal solution on the two axes: $\boldsymbol{s}_{\mathrm{IP}}$ and $\boldsymbol{s}_{\mathrm{OP}}$. Here, we have to note that the measured points (circles) are not on a straight line, but on a curve as schematically illustrated in Figure 5. This means that a choice of some points largely influences the extrapolated results.

For example, if the three open circles are chosen, the extrapolated solutions on the 0° and 90° axes yield $\boldsymbol{s}_{\mathrm{IP}}$ and $\boldsymbol{s}_{\mathrm{OP}}$, but the norm (distance from the origin) of the two vectors are apparently different from each other, which means that the ordinate scales of the IP and OP spectra are different from each other.

If the three closed circles are chosen, on the other hand, the IP and OP spectra obtained in the extrapolated manner have a common ordinate scale. In this case, therefore, the three angles of incidence represented by the three closed circles are the optimal angles of incidence for the pMAIRS measurements. In this manner, optimization of the angles of incidence is key to accomplish pMAIRS as a practically useful quantitative analytical technique.

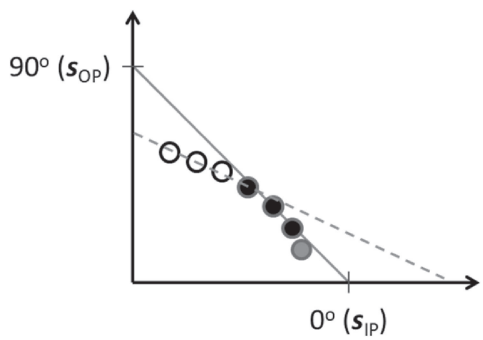

Figure 5. Experimental optimization by choosing an appropriate set (closed circles) of incident angles. The two orthogonal axes correspond to the direction of $\boldsymbol{s}_{\mathrm{IP}}$ and $\boldsymbol{s}_{\mathrm{OP}}$.

6. Optimization of pMAIRS

Determination of the optimal angles of incidence is necessary to make pMAIRS quantitatively useful, but it is a difficult task indeed. At an early stage of the pMAIRS development, a thin film of highly oriented molecules was used as the calibration standard, so that the band intensity ratio of the IP spectrum to the OP spectrum would agree with the orientation angle known in advance.[11] This calibration technique based on band 'intensity' requires a highly reliable standard sample with the oriented molecules, which is not practical for many users.

To overcome the experimental difficulties, a totally different approach is employed: band 'position' is used for the calibration. When strongly IR absorbing molecules are close to each other, a lattice or cluster of dipole-dipole interacting aggregates absorbs IR ray in place of a single molecule, which would be in a phonon or polariton state.[12–14] In this state, degenerated phonon modes are split into the transverse and longitudinal optic (TO and LO, respectively) waves, which is called the TO-LO splitting.[12–14] The TO-LO splitting does occur not only for a crystal, but also for an amorphous matter involving glass and liquid.[15]

For the use of the TO-LO splitting for the calibration, perfluoroalkyl (R_f)-containing compounds are useful. An R_f group composed of the C–F bonding has a large permanent dipole moment at each bond,[16] which works as a strong IR absorber inducing the TO-LO splitting.[1,14,15] When the R_f group is $(CF_2)_6$ or shorter, the spontaneous molecular aggregation is weak,[17,18] and as a result, the compound is liquid or gas at ambient temperature, i.e., a structurally isotropic matter. Band positions of the TO and LO modes are obtained from the attenuated total reflection (ATR) spectrum of the isotropic R_f-containing compound by using the Kramers-Kronig relationship.[1,17,19] Therefore, what we have to do is determination of appropriate angles of incidence, so that the shape of a pMAIRS spectrum would match that of the calculated TO and LO spectra.

For details of this procedure, the reader is referred to a reference.[20] Here, the optimal conditions are presented in Table 1. The optimal angles of incidence depend on the refractive index of the substrate, n_{sub}, used for the thin-film support. For example, when using a silicon (Si) substrate, we have to take the angles of incidence from 9 to 44° by 5° steps, i.e., eight single-beam spectra in total, for both S and B measurements.

7. Molecular Orientation Analysis Using pMAIRS

If the ordinate scales of the IP and OP spectra were ideally made common, the simple band intensity ratio would yield the orientation angle of the transition moment (eq 8).

$$\phi = \tan^{-1}\sqrt{\frac{2A_{\mathrm{IP}}}{A_{\mathrm{OP}}}} \tag{8}$$

The orientation analysis of eq 8 has a powerful benefit that analytical accuracy of the molecular orientation is robust to the

Table 1. Optimal experimental parameters for representative IR transparent substrates, on which a thin film is deposited

Substrate	n_{sub}	Angles of incidence/°	Angle step/°	H
Ge	4.0	9–44	5	0.15
Si	3.4	9–44	5	0.14
ZnSe	2.4	9–44	5	0.13[a]
CaF_2	1.4	8–38	6	0.21

[a]In the original paper, the value of ZnSe was miscalculated to be 0.11.

surface roughness of the film. This is because the roughness influences equally to both IP and OP spectra, which is cancelled by making the intensity ratio.

Nonetheless, when a thin film of a spherical molecule of fullerene (C_{60}) is measured by pMAIRS, unfortunately, the OP spectrum appears with an entirely larger intensity than the IP spectrum.[21] Since C_{60} is an intrinsically isotropic compound, all the bands must exhibit an isotropic result: $A_{IP} = A_{OP}$. Therefore, this disagreement implies that the pMAIRS technique still has an inaccuracy even after the experimental optimization.

The reason of the inaccuracy is that the 'refractive index of the thin film' influences the A_{IP} and A_{OP} spectra in a different manner. To make both spectra have an ideally common scale, an additional correction is necessary, which is called "n^4H correction."[21] This correction on a condition of $n^2 \gg k^2$ works well when:

1) The refractive index of the thin film is apparently far from that of usual organic matter located at ca. $n = 1.55$. The typical examples are C_{60} ($n = 1.8$ or higher) and R_f compounds ($n =$ 1.4 or less), and

2) The refractive index of the substrate is lower than $n_{sub} =$ 2.5, which is typically found for CaF_2.

In these cases, we have to correct the ordinate scale (eq 9) by using a substrate-specific factor, H, as well as n as found in Table 1.

$$\phi = \tan^{-1}\sqrt{\frac{2A_{IP}}{n^4H \cdot A_{OP}}} \tag{9}$$

Fortunately, eq 9 readily explains why the conventional many pMAIRS spectra gave reasonable results without using the correction. In fact, a usual organic material with $n = 1.6$ deposited on a Si substrate ($n_{sub} = 3.4$; $H = 0.14$) yields $n^4H = 0.92 \approx 1$. We have to note, however, that the correction term is essentially necessary for the measurements of pMAIRS spectra.

Fortunately, this correction using the parameters in Table 1 is involved in the commercial pMAIRS equipment, and the operation is quite easily done as a black box.

We are now ready to use pMAIRS for practical applications. Figure 6 presents a pMAIRS spectrum of a pentacene (PEN) film deposited by an evaporation technique on a Si substrate. A single pMAIRS spectrum consists of two spectra of the IP and OP spectra presented by the red and blue curves, respectively.

PEN is a stiff molecule that has three mutually orthogonal normal modes along the short- and long-axes as well as the plane normal, which are denoted as x, y and z, respectively, and they appear at largely different band positions. By measuring

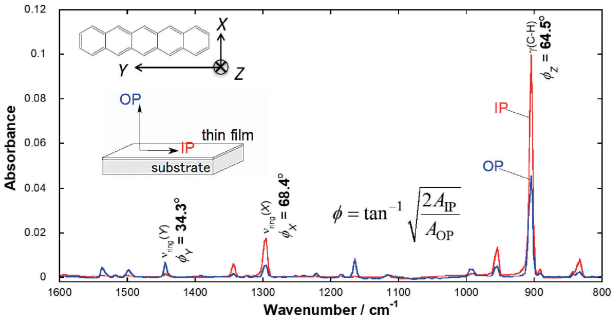

Figure 6. A pMAIRS spectrum of a PEN film deposited on a Si substrate.

the band intensity ratio of each band, the orientation angles from the surface normal are easily calculated as shown in the figure.

When a set of three mutually orthogonal directions are considered, the tilt angles of the directions measured from a common direction satisfy the direction-cosine equation (eq 10) in theory.[1,2,4,6]

$$\cos^2\phi_x + \cos^2\phi_y + \cos^2\phi_z = 1 \tag{10}$$

When the three orientation angles are put in this equation, in fact, the summation is 1.00. This surprisingly beautiful result straightforwardly implies that the analytical accuracy of pMAIRS attains three significant digits. One of the reasons of the high accuracy is that only the p-polarization is used: the polarization dependency of FT-IR is excluded.

This accuracy check using eq 10 is quite convenient to examine whether the pMAIRS spectra are properly measured or not. If there is a problem with the sample or with the spectrometer, the summation becomes far from unity. For example, if the surface roughness is measured by atomic force microscope (AFM) to have a root mean square (RMS) roughness of more than 100 nm, the summation of the direction cosines tends to be far from unity by more than 10%.

8. Application Studies Using pMAIRS

One of the most useful application targets of pMAIRS is organic electronics, which requires analysis and control of molecular orientation for developing high-performance organic thin-film devices as found over more than two decades.[22–63] The molecular orientation in an organic semiconductor thin film is analyzed by using various characterization tools such as 2D-GIXD,[64–67] electron diffraction (ED),[68,69] near-edge X-ray absorption fine structure (NEXAFS),[65,70] spectroscopic ellipsometry (SE),[51,71] polarized Raman[72–75] and vibrational sum-frequency generation (SFG)[76–79] spectroscopies. Many recent papers, in addition, demonstrate that pMAIRS works effectively as an alternative technique for revealing the molecular arrangement in organic semiconductor thin films,[80–92] as shown in the following sections. Note that pMAIRS can easily be installed on FT-IR, and it provides rich chemical information not only of molecular orientation, but of conformation, molecular packing and even polymorphs in a thin film with a surface roughness.

A) Molecular Orientation Analysis Irrespective of Crystallinity. High-crystalline materials are of a two-dimension-

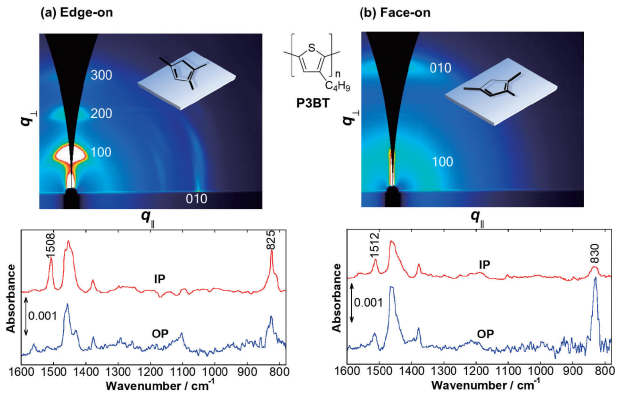

Figure 7. 2D-GIXD patterns (upper panel) and pMAIRS spectra (lower panel) of P3BT thin films having two different orientations ((a) edge-on and (b) face-on configurations) deposited on a Si substrate.

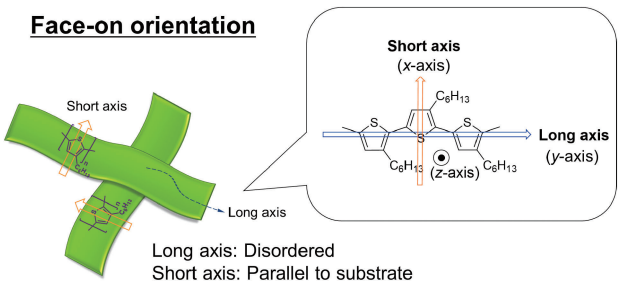

Figure 8. Schematic illustrations of a face-on orientation of P3AT in a thin film.

ally well-organized molecular assembly on a solid surface in general, but this does not mean that an amorphous part has a random orientation. Yokoyama and co-workers report that several amorphous materials for organic light-emitting diodes (OLEDs) tend to be oriented horizontally in the film, and the order of orientation significantly influences the device performance.[25,51] In a similar manner, for organic photovoltaics (OPVs) using semi-crystalline polymers, molecular orientation is recognized to be one of the critical parameters for enhancing the power conversion efficiency.[30,32,33,39,45,49] Analysis of molecular orientation in a low-crystalline film is thus of great interest particularly for developing OLEDs and OPVs. For this purpose, pMAIRS works powerfully showing an outstanding performance for the quantitative analysis as follows.

The most widely used material for OPVs, poly(3-alkylthiophene) (P3AT),[93–95] works as an excellent p-type semiconductor even with a low crystallinity. Although the aptitude has already been studied well depending on the molecular arrangement, a fully molecular schematic is not at hand. By using the pMAIRS technique, we have revealed the accurate molecular structure and the controlling mechanism of molecular orientation.[90,92]

To discuss the relationship between the molecular orientation and the crystallinity, two crystallinity-controlled films of poly(3-butylthiophene) (P3BT) are compared (for preparation, see the original paper[90]). The 2D-GIXD patterns of the two films are presented in Figure 7. The strong (h00) reflections due to the lamellar structure appear along the $q_\perp$ axis in Figure 7a where $q_\perp$ is the OP component of the scattering vector. This indicates that the edge-on orientation is formed in the crystalline lamellae, since the crystallographic a-axis is along the alkyl side chains (i.e., x-axis; Figure 8). The other film has almost no lamellar peaks (Figure 7b), and a broad halo indexed as 010 is observed in the high $q_\perp$ region. This is a typical diffraction pattern of liquid-crystalline thin films,[96] and it is further evidence of having no lamellar crystalline structure. On the GIXD pattern alone, in this manner, quantitative orientation analysis of a low crystalline material is difficult.

The pMAIRS spectra, on the other hand, show an apparent difference of the intensity ratio of IP and OP bands at about 825 cm^{-1}. This band is assigned to the C–H out-of-plane deformation vibration (denoted as γ(C–H)) mode of the π-conjugated skeleton.[97] This band appears strongly in the IP spectrum for the film (Figure 7a); whereas it appears strongly in the OP spectrum for the film (Figure 7b). Since the transition dipole moment is directed normal to the ring plane (z-axis; Figure 8), the relatively strong IP and OP bands roughly mean the edge-on and face-on orientations, respectively, in the film.[90,92] With this surface selection rule, the higher crystalline film is confirmed to have the edge-on crystallites predominantly. On the contrary, for the other one, the face-on orientation is preferentially formed. Because the GIXD pattern has no lamellar peaks, the face-on orientation is thus found not driven by the intermolecular interaction. This experimental result is consistent with a previous paper[98] using molecular dynamics (MD) simulations reporting that a single molecule of P3AT prefers a face-on configuration induced by the molecule-substrate interaction.

Another notable observation is that the ring stretching vibration[97] band appeared at 1512 cm^{-1} has an intensity ratio of nearly unity for the face-on thin film (Figure 7b). By carefully analyzing the band as well as the γ(C–H) band, the face-on orientation of P3AT is found to be defined by the highly aligned molecular short-axis as depicted in Figure 8.[92] At the same time, the long-axis is relatively disordered. In this manner, pMAIRS has a powerful benefit that quantitative orientation analysis can be performed for each chemical group, as further mentioned below.

B) Molecular Orientation Analysis of Each Chemical Group. Another interesting application of pMAIRS is shown for solution-processed zinc tetraphenylporphyrin (ZnTPP; Figure 9a) thin films.[91] ZnTPP has four phenyl rings attached to the porphyrin skeleton, and the phenyl rings typically take a twisted conformation to the porphyrin ring due to steric hindrance. The phenyl rings contribute to its high solubility in general organic solvents, which makes the solution-coating techniques possible. Although the spin-coated films of ZnTPP and its related compounds are practically used in various organic thin-film devices such as OPVs[99,100] and organic sensors,[101–103] a comprehensive understanding of the structure-controlling factors is inadequate.

In the original paper,[91] influences of the three factors of solvent, coating technique, and thermal annealing on the molecular structure in the film are discussed. As a result, the evaporation time of solvent is found to be key, which can easily be controlled by changing the solvent and the coating technique. For example, the combination of chloroform (Chl) and spin-coating (SC) results in the shortest evaporation time for obtain-

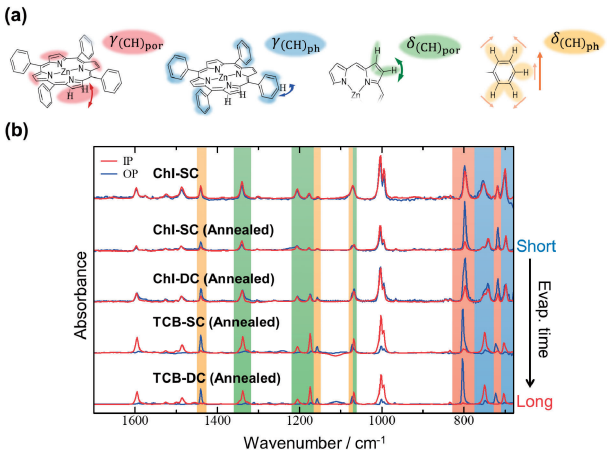

Figure 9. (a) Schematics of chemical structure and some representative vibrational modes of ZnTPP. (b) pMAIRS spectra of ZnTPP thin films deposited on a Si substrate.

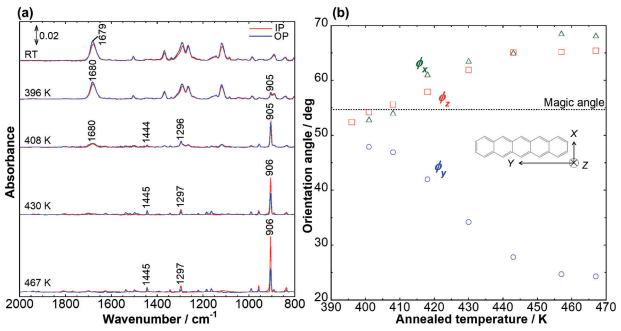

Figure 10. (a) pMAIRS spectra of solution-processed PEN thin films, and (b) the calculated orientation angles as a function of the annealed temperature.

ing the film (Chl-SC film). The pMAIRS spectrum of the Chl-SC film indicates a nearly perfect random orientation judging from the good agreement of the IP and OP spectra over the entire wavenumber range (Figure 9b). In contrast, the combination of the longest evaporation time of solvent, that is, 1,2,4-trichlorobenzene and drop-casting (TCB-DC) induces a remarkably ordered polycrystalline structure in the film regardless of thermal annealing. The annealed film, in particular, shows an extremely high dichroic ratio in Figure 9b.

Here, we have to note that pMAIRS works powerfully for discussing the molecular orientations of the porphyrin and phenyl rings individually, which is difficult by using other techniques. These two rings exhibit a contrasting intensity ratio in the spectra, as typically found for the γ(C–H) bands in Figure 9b. As a result, the porphyrin ring is found to be oriented in a face-on manner, while the phenyl ones take the edge-on configuration. Analytical details are referred to the original paper.[91] Of another note is that the degree of orientation becomes higher as the evaporation time increases. In this way, quantitative analysis of each chemical group by pMAIRS is quite useful for discussing the relationship between the film-preparation parameters and the molecular orientation of ZnTPP systematically.

C) Three-Dimensional Orientation Analysis. Next, we show another useful characteristic of pMAIRS, which is used for analysis of a solution-processed PEN thin film.[81] The film can be prepared by the thermal conversion technique using a soluble precursor (13,6-*N*-sulfinylacetamidopentacene; SAP).[104] As described in Section 7, PEN has three mutually orthogonal normal modes (see the molecular scheme in Figure 6),[105] which give absorption bands at 1445, 1297 and 906 cm^{-1} in the spectra (Figures 6 and 10a). The intensity ratio of the IP to OP bands directly gives the quantitative orientation angle for the three orthogonal modes using eq 8. This is an outstanding advantage when comparing to other spectroscopic techniques such as ultraviolet-visible (UV-Vis) absorption spectrometry and NEXAFS.

The calculated orientation angles (ϕ_x, ϕ_y and ϕ_z) give the three-dimensional (3D) orientation image of the molecule against the thermal-treatment temperature in Figure 10b. The plot indicates that all the angles are at near the magic angle (54.7°) immediately after beginning of the thermal conversion. In other words, PEN is randomly oriented in the film at an early stage of the structural conversion process. The 3D orientation analysis is a unique property of pMAIRS, and even the NEXAFS technique cannot depict the 3D structure of PEN, because the technique provides only orientation information of the *z*-axis, i.e., ϕ_z.[70]

9. Advanced Analysis Using pMAIRS

As shown in Section 8, pMAIRS exhibits highly useful performance as a structural characterization tool for organic thin films. pMAIRS has, in fact, high potential for structural characterization of thin-film samples, not only to the molecular orientation analysis. In this section, a totally different use of pMAIRS is shown as follows.

A) Another Use of pMAIRS: Quantity Analysis in a Film. Quantitative analysis of chemical constituents in a thin film using spectroscopy with the aid of multivariate techniques (i.e., chemometrics) is a challenging long-term issue in analytical spectroscopy. This is because the spectral intensity (absorbance) of a thin film is influenced not only by the quantity, but also by the molecular orientation via the surface selection rules. If the influence of molecular orientation can be removed, the spectral intensity would be governed by only the quantity of constituents in the film. This is realized by using the pMAIRS technique.[81]

Here, we note again that both IP and OP spectra have a common ordinate scale. With this characteristic, pMAIRS can uniquely annihilate the influence of the molecular orientation by simply taking the average of A_{IP} and A_{OP} to generate the isotropic spectrum, A_{iso} (eq 11).[81]

$$A_{iso} = \frac{1}{3}(2A_{IP} + A_{OP}) \tag{11}$$

The isotropic spectrum is a spectrum, as if it were measured on an orientation-free (perfectly random) film. Of course, the quantity information of all the constituents in the film is readily preserved in A_{iso}.

In this manner, the pMAIRS-IP and -OP spectra can now be used in two totally different ways: i) molecular orientation is calculated by taking the ratio, and ii) molecular orientation is annihilated to leave the quantity only by taking the average of the spectra, which is schematically summarized in Figure 11a.

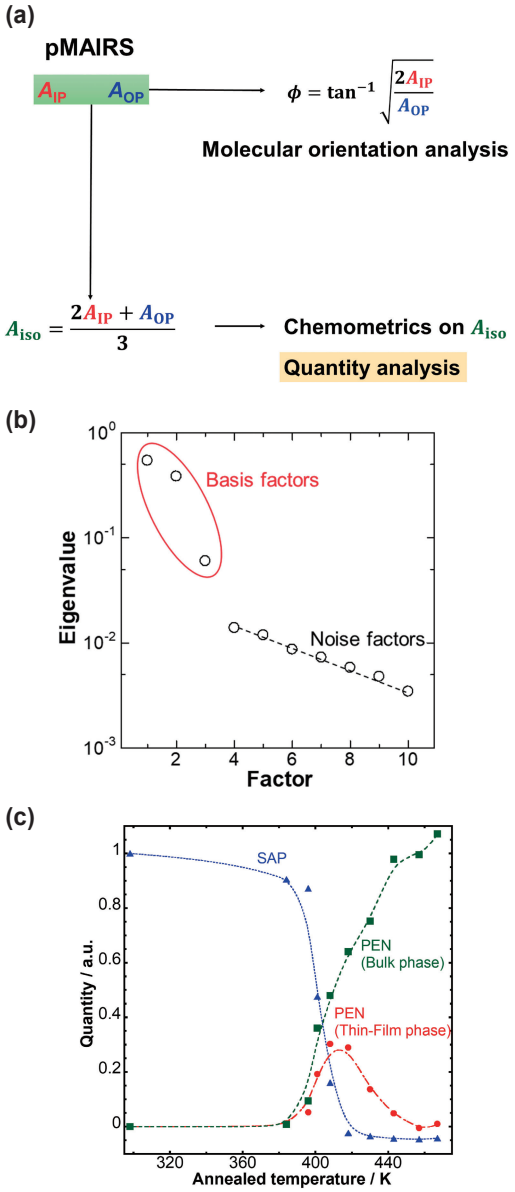

Figure 11. (a) Schematic summary of two different uses of pMAIRS. (b) Eigenvalue plot after the PCA analysis of A_{iso} of a SAP/PEN film and (c) an analytical result by the CLS regression calculation.

Once the influence of orientation is removed, the isotropic spectra can directly be used for chemometric analysis.

As an example, the CLS regression technique can be coupled with pMAIRS for revealing quantity changes of the chemical species involved in the film during the thermal conversion process of SAP to PEN.[81] Before the CLS analysis, the isotropic spectra measured at various annealed temperatures, A_{iso}, were subjected to the principal component analysis (PCA).[1] The eigenvalue plot is presented in Figure 11b. An eigenvalue plot of a collection of spectra of a thin film often yields an ambiguous result having no apparent boundary between the basis and noise factors. Figure 11b shows, however, an ideally beautiful eigenvalue plot, from which we can determine that the number of constituents is apparently three. This clear PCA analysis straightforwardly implies that the isotropic spectra on pMAIRS are powerful for chemometric analysis.

The 'three' constituents go to SAP and two crystalline phases of PEN, i.e., the thin film and bulk phases.[81] These three phases can strictly be discriminated by means of IR spectroscopy.

Then, the CLS analysis was performed on A_{iso} by the use of the three pure-component spectra. The analytical results are presented in Figure 11c. The plot clearly shows that the reactant of SAP mostly disappears at 420 K, and instead the thin-film and bulk phases of PEN appear and grow together. At a higher temperature, the thin-film phase is rearranged into the bulk phase.

B) Visible-pMAIRS Analysis Monitors Davydov Splitting. pMAIRS is mostly employed for the IR region, but it has more versatility. Here, an example of using pMAIRS coupled with UV-vis spectroscopy (Vis-pMAIRS) is shown.[106,107] Vis-pMAIRS reveals the anisotropic electronic absorptions in a thin film, which are substantially related to the charge transport in the film. In this sense, Vis-pMAIRS should be a promising analytical tool to study the structure-property relationship for optoelectronic devices. In addition, this technique also gives insight into the molecular orientation of organic semiconductors in a thin film, from a different perspective of IR-pMAIRS.

Control of the molecular orientation of PEN on a dielectric material is a challenging topic. This compound is spontaneously aggregated to have end-on orientation on the supporting substrate at ambient temperature.[108] This is due to the high aggregation property and the anisotropic molecular shape of PEN.[108,109] According to a study using MD-simulations,[110] on the other hand, a single molecule of PEN takes the face-on stance on amorphous SiO_2. A low-temperature (LT) deposition technique is thus a candidate for realizing the face-on oriented film, since the surface diffusion of a molecule is kinetically restricted on a cold substrate.[71,96,111–113] In the past, PEN was believed to take a randomly oriented amorphous structure in LT film.[114–117] PEN thin films at ambient temperature were known to exhibit Davydov splitting in the visible region due to herring-bone crystalline packing, but it was not observed for the LT film.[116,117] This implies that no crystalline aggregates were generated in the LT film. This interpretation has long been believed to be true of the molecular structure in the LT film. We have to note, however, that the conventional spectra were measured by the normal-incidence Tr technique only.

By using the Vis-pMAIRS technique, the OP absorption spectrum is first obtained for the LT film (the blue curve in Figure 12a),[86] where the IP spectrum (red curve) reproduces the conventionally measured Tr spectrum. In the Vis-pMAIRS spectra, the two Davydov components at 1.86 and 1.98 eV appear individually in the IP and OP spectra, respectively. Considering the direction of the transition moments, the molecule should be aligned with the face-on orientation as depicted in Figure 12b.[86] In this way, Vis-pMAIRS readily makes up for the OP spectrum that has long been missed, which largely corrects the conventional interpretation by finding the Davydov splitting.

10. MAIRS2: A New Generation of MAIRS

The pMAIRS technique is widely employed for various organic compounds ranging from polymers to low-molecular-

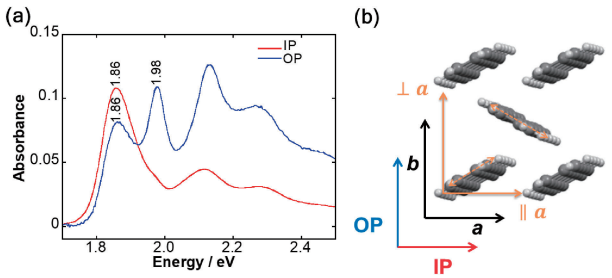

Figure 12. (a) Vis-pMAIRS spectra of a PEN LT film, and (b) the thin film structure revealed.

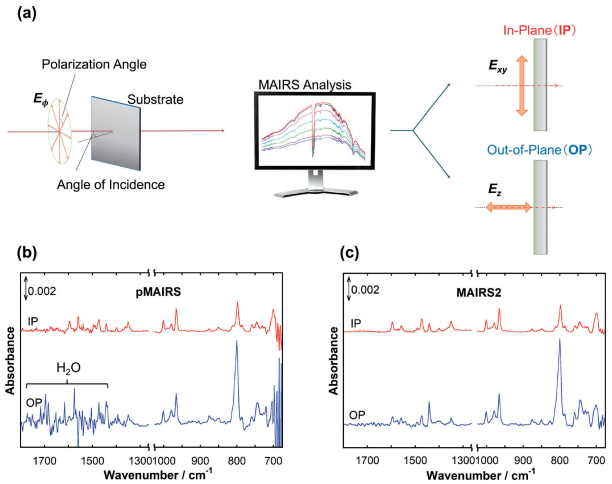

Figure 13. (a) Schematic of MAIRS2 measurements and analysis of a thin film. The (b) pMAIRS and (c) MAIRS2 spectra of a tetraphenylporphyrin thin film on Si.

weight materials as mentioned above. Sometimes, nevertheless, unexpected noise components interfere with the analysis. The most representative one is interference fringes due to the multiple reflections of light within the substrate. The other is water-vapor peaks deformed through the double FT modulation of IR ray involving the reflected ray from the substrate.[118] These measurement troubles are especially severe for low angle ($\theta <$ 10°) incidence measurements. Unfortunately, pMAIRS measurements are on the multiple-angle measurements including a low angle of incidence.[20]

To overcome the problem, an alternative MAIRS technique has recently been developed,[118] which is called "MAIRS2." The different points from pMAIRS are summarized:

1) The angle of incidence is fixed at a specific angle determined by the substrate material (for example, 45° for Si). Instead, the polarization angle is changed from 0° to 90° during the measurements as schematically shown in Figure 13a.
2) The ***R*** matrix of the MAIRS analysis is changed to have a polarization-angle-dependent form (see the original paper).

This is a simple modification of the measurement process indeed, but it improves the obtained results drastically, particularly for the OP spectrum, as found in Figure 13c. The noisy water-vapor peaks in Figure 13b are beautifully removed. MAIRS2 is indeed powerful and useful for many IR users, since we do not have to worry about the optical fringes that appear not only in MAIRS spectra, but on Tr spectra. Since the rotation of the sample stage is not needed during the measurements, MAIRS2 would be a basic technology to develop MAIRS for further applications.

Note that, however, MAIRS2 cannot be used for analysis of a biaxially oriented sample, since the linear polarizer is rotated during the measurements.

11. Conclusion

MAIRS equipped FT-IR is now a practically useful and powerful technique for analysis of the thin-film structure represented by molecular orientation using very few parameters in advance such as the refractive index of the film. Other parameters are automatically set by choosing the substrate material, and the user can use it as a black box. Since the orientation anlaysis is robust to the surface roughness of the film, MAIRS is superior to other spectroscopic techniques. The two options of pMAIRS and MAIRS2 are conveniently used up to the analytical purposes. MAIRS2 frees us from the concerns of water-vapor peaks and optical fringes, whereas pMAIRS is easy to introduce into the laboratory and it works for analysis not only of uniaxial orientation distribution, but of biaxial orientation in the film. MAIRS on FT-IR is a complementary technique to GIXD for full understanding of a thin film, which should boost research on a thin film or molecular adsorbates on a solid surface including fluorous chemistry[119–122] and medical applications[123] and others.[124–128]

The 2D-GIXD measurements were performed at the BL46XU beamline of SPring-8 with the approval of the Japan Synchrotron Radiation Research Institute (JASRI) (Proposal No. 2017B1831). The authors thank Prof. Hiroyuki Yoshida and Tomoyuki Koganezawa for help for the GIXD experiments.

References

1 T. Hasegawa, *Quantitative Infrared Spectroscopy for Understanding of a Condensed Matter*, Springer, Tokyo, 2017.
2 M. S. Dresselhaus, G. Dresselhaus, A. Jorio, *Group Theory: Application to the Physics of Condensed Matter*, Springer, Berlin, 2008.
3 M. Tasumi, *Introduction to Experimental Infrared Spectroscopy*, Wiley, Chichester, 2015.
4 V. P. Tolstoy, I. V. Chernyshova, V. A. Skryshevsky, *Handbook of Infrared Spectroscopy of Ultrathin Films*: Wiley, Chichester, UK, 2003.
5 R. G. Greenler, *J. Chem. Phys.* **1966**, *44*, 310.
6 T. Hasegawa, S. Takeda, A. Kawaguchi, J. Umemura, *Langmuir* **1995**, *11*, 1236.
7 T. Hasegawa, *J. Phys. Chem. B* **2002**, *106*, 4112.
8 Y. Itoh, A. Kasuya, T. Hasegawa, *J. Phys. Chem. A* **2009**, *113*, 7810.
9 T. Hasegawa, Y. Nakano, Y. Ishii, *Anal. Chem.* **2006**, *78*, 1739.
10 T. Hasegawa, *Anal. Chem.* **2007**, *79*, 4385.
11 T. Hasegawa, Y. Itoh, A. Kasuya, *Anal. Sci.* **2008**, *24*, 105.
12 V. M. Agranovich, D. L. Mills, *Surface Polaritons: Electromagnetic Waves at Surfaces and Interfaces*: North-Holland Publishing Company, Amesterdam, The Netherlands, 1982.
13 Y. Toyozawa, *The Physics of Elementary Excitations*,

edited by S. Nakajima,Y. Toyozawa, and R. Abe, Springer-Verlag, Berlin, 1980.
14 N. Nagai, H. Okada, T. Hasegawa, *AIP Adv.* **2019**, *9*, 105203.
15 K. Yamamoto, A. Masui, *Appl. Spectrosc.* **1996**, *50*, 759.
16 T. Hasegawa, *Chem. Phys. Lett.* **2015**, *627*, 64.
17 T. Hasegawa, T. Shimoaka, N. Shioya, K. Morita, M. Sonoyama, T. Takagi, T. Kanamori, *ChemPlusChem* **2014**, *79*, 1421.
18 T. Hasegawa, *Chem. Rec.* **2017**, *17*, 903.
19 J. S. Plaskett, P. N. Schatz, *J. Chem. Phys.* **1963**, *38*, 612.
20 N. Shioya, S. Norimoto, N. Izumi, M. Hada, T. Shimoaka, T. Hasegawa, *Appl. Spectrosc.* **2016**, *71*, 910.
21 N. Shioya, T. Shimoaka, R. Murdey, T. Hasegawa, *Appl. Spectrosc.* **2017**, *71*, 1242.
22 K. Yamada, M. Okamoto, M. Sakurai, T. Suenobu, K. Nakayama, *RSC Adv.* **2019**, *9*, 32940.
23 Y. Watanabe, H. Sasabe, J. Kido, *Bull. Chem. Soc. Jpn.* **2019**, *92*, 716.
24 K. Yamada, K. Nakayama, *J. Electrochem. Soc.* **2019**, *166*, B3103.
25 Y. Watanabe, D. Yokoyama, T. Koganezawa, H. Katagiri, T. Ito, S. Ohisa, T. Chiba, H. Sasabe, J. Kido, *Adv. Mater.* **2019**, *31*, 1808300.
26 F. Wang, K. Hashimoto, H. Segawa, K. Tajima, *ACS Appl. Mater. Interfaces* **2018**, *10*, 8901.
27 S. Jinnai, Y. Ie, Y. Kashimoto, H. Yoshida, M. Karakawa, Y. Aso, *J. Mater. Chem. A* **2017**, *5*, 3932.
28 N. A. Ran, S. Roland, J. A. Love, V. Savikhin, C. J. Takacs, Y.-T. Fu, H. Li, V. Coropceanu, X. Liu, J.-L. Brédas, G. C. Bazan, M. F. Toney, D. Neher, T.-Q. Nguyen, *Nat. Commun.* **2017**, *8*, 79.
29 A. Hamidi-Sakr, L. Biniek, S. Fall, M. Brinkmann, *Adv. Funct. Mater.* **2016**, *26*, 408.
30 J. W. Jo, J. W. Jung, H. Ahn, M. J. Ko, A. K.-Y. Jen, H. J. Son, *Adv. Energy Mater.* **2017**, *7*, 1601365.
31 Y. Shimata, M. Ide, M. Tashiro, M. Katouda, Y. Imamura, A. Saeki, *J. Phys. Chem. C* **2016**, *120*, 17887.
32 B. Kitchen, O. Awartani, R. J. Kline, T. McAfee, H. Ade, B. T. O'Connor, *ACS Appl. Mater. Interfaces* **2015**, *7*, 13208.
33 C. Lu, H.-C. Chen, W.-T. Chuang, Y.-H. Hsu, W.-C. Chen, P.-T. Chou, *Chem. Mater.* **2015**, *27*, 6837.
34 H.-C. Lin, G. A. MacDonald, Y. Shi, N. W. Polaske, D. V. McGrath, S. R. Marder, N. R. Armstrong, E. L. Ratcliff, S. S. Saavedra, *J. Phys. Chem. C* **2015**, *119*, 10304.
35 G. O. N. Ndjawa, K. R. Graham, R. Li, S. M. Conron, P. Erwin, K. W. Chou, G. F. Burkhard, K. Zhao, E. T. Hoke, M. E. Thompson, M. D. McGehee, A. Amassian, *Chem. Mater.* **2015**, *27*, 5597.
36 I. Osaka, K. Takimiya, *Polymer* **2015**, *59*, A1.
37 U. Hörmann, C. Lorch, A. Hinderhofer, A. Gerlach, M. Gruber, J. Kraus, B. Sykora, S. Grob, T. Linderl, A. Wilke, A. Opitz, R. Hansson, A. S. Anselmo, Y. Ozawa, Y. Nakayama, H. Ishii, N. Koch, E. Moons, F. Schreiber, W. Brütting, *J. Phys. Chem. C* **2014**, *118*, 26462.
38 A. L. Ayzner, D. Nordlund, D.-H. Kim, Z. Bao, M. F. Toney, *J. Phys. Chem. Lett.* **2015**, *6*, 6.
39 J. R. Tumbleston, B. A. Collins, L. Yang, A. C. Stuart, E. Gann, W. Ma, W. You, H. Ade, *Nat. Photonics* **2014**, *8*, 385.
40 L. Zhang, S. S. Roy, R. J. Hamers, M. S. Arnold, T. L. Andrew, *J. Phys. Chem. C* **2015**, *119*, 45.
41 M. Aghamohammadi, A. Fernández, M. Schmidt, A. Pérez-Rodríguez, A. R. Goñi, J. Fraxedas, G. Sauthier, M. Paradinas, C. Ocal, E. Barrena, *J. Phys. Chem. C* **2014**, *118*, 14833.
42 H.-R. Tseng, H. Phan, C. Luo, M. Wang, L. A. Perez, S. N. Patel, L. Ying, E. J. Kramer, T.-Q. Nguyen, G. C. Bazan, A. J. Heeger, *Adv. Mater.* **2014**, *26*, 2993.
43 J. Ma, K. Hashimoto, T. Koganezawa, K. Tajima, *Chem. Commun.* **2014**, *50*, 3627.
44 K. R. Graham, P. Erwin, D. Nordlund, K. Vandewal, R. Li, G. O. N. Ndjawa, E. T. Hoke, A. Salleo, M. E. Thompson, M. D. McGehee, A. Amassian, *Adv. Mater.* **2013**, *25*, 6076.
45 X. Guo, N. Zhou, S. J. Lou, J. Smith, D. B. Tice, J. W. Hennek, R. P. Ortiz, J. T. L. Navarrete, S. Li, J. Strzalka, L. X. Chen, R. P. H. Chang, A. Facchetti, T. J. Marks, *Nat. Photonics* **2013**, *7*, 825.
46 T. Mizokuro, Y. Okamoto, C. Heck, H. Aota, N. Tanigaki, *J. Appl. Polym. Sci.* **2013**, *131*, 40136.
47 D. T. James, J. M. Frost, J. Wade, J. Nelson, J.-S. Kim, *ACS Nano* **2013**, *7*, 7983.
48 B. P. Rand, D. Cheyns, K. Vasseur, N. C. Giebink, S. Mothy, Y. Yi, V. Coropceanu, D. Beljonne, J. Cornil, J.-L. Brédas, J. Genoe, *Adv. Funct. Mater.* **2012**, *22*, 2987.
49 S. Shao, J. Liu, J. Zhang, B. Zhang, Z. Xie, Y. Geng, L. Wang, *ACS Appl. Mater. Interfaces* **2012**, *4*, 5704.
50 A. Ojala, A. Petersen, A. Fuchs, R. Lovrincic, C. Pölking, J. Trollmann, J. Hwang, C. Lennartz, H. Reichelt, H. W. Höffken, A. Pucci, P. Erk, T. Kirchartz, F. Würthner, *Adv. Funct. Mater.* **2012**, *22*, 86.
51 D. Yokoyama, *J. Mater. Chem.* **2011**, *21*, 19187.
52 W. Chen, D.-C. Qi, H. Huang, X. Gao, A. T. S. Wee, *Adv. Funct. Mater.* **2011**, *21*, 410.
53 D. M. Alloway, N. R. Armstrong, *Appl. Phys.* **2009**, *95*, 209.
54 M. He, J. Li, M. L. Sorensen, F. Zhang, R. R. Hancock, H. H. Fong, V. A. Pozdin, D.-M. Smilgies, G. G. Malliaras, *J. Am. Chem. Soc.* **2009**, *131*, 11930.
55 S. Duhm, G. Heimel, I. Salzmann, H. Glowatzki, R. L. Johnson, A. Vollmer, J. P. Rabe, N. Koch, *Nat. Mater.* **2008**, *7*, 326.
56 H.-W. Lin, C.-L. Lin, C.-C. Wu, T.-C. Chao, K.-T. Wong, *Org. Electron.* **2007**, *8*, 189.
57 D. M. DeLongchamp, B. M. Vogel, Y. Jung, M. C. Gurau, C. A. Richter, O. A. Kirillov, J. Obrzut, D. A. Fischer, S. Sambasivan, L. J. Richter, E. K. Lin, *Chem. Mater.* **2005**, *17*, 5610.
58 M. Misaki, Y. Ueda, S. Nagamatsu, M. Chikamatsu, Y. Yoshida, N. Tanigaki, K. Yase, *Appl. Phys. Lett.* **2005**, *87*, 243503.
59 D. M. DeLongchamp, S. Sambasivan, D. A. Fischer, E. K. Lin, P. Chang, A. R. Murphy, J. M. J. Fréchet, V. Subramanian, *Adv. Mater.* **2005**, *17*, 2340.
60 J.-F. Chang, B. Sun, D. W. Breiby, M. M. Nielsen, T. I. Sölling, M. Giles, I. McCulloch, H. Sirringhaus, *Chem. Mater.* **2004**, *16*, 4772.
61 T. Virgili, D. G. Lidzey, M. Grell, D. D. C. Bradley, S. Stagira, M. Zavelani-Rossi, S. D. Silvestri, *Appl. Phys. Lett.* **2002**, *80*, 4088.
62 C. Videlot, A. E. Kassmi, D. Fichou, *Sol. Energy Mater. Sol. Cells* **2000**, *63*, 69.
63 H. Sirringhaus, P. J. Brown, R. H. Friend, M. M. Nielsen, K. Bechgaard, B. M. W. Langeveld-Voss, A. J. H. Spiering, R. A. J. Janssen, E. W. Meijer, P. Herwig, D. M. de Leeuw, *Nature* **1999**, *401*, 685.
64 N. Widjonarko, *Coatings* **2016**, *6*, 54.
65 J. Rivnay, S. C. B. Mannsfeld, C. E. Miller, A. Salleo, M. F. Toney, *Chem. Rev.* **2012**, *112*, 5488.

66 J. L. Baker, L. H. Jimison, S. Mannsfeld, S. Volkman, S. Yin, V. Subramanian, A. Salleo, A. P. Alivisatos, M. F. Toney, *Langmuir* **2010**, *26*, 9146.
67 M. L. Chabinyc, *Polym. Rev.* **2008**, *48*, 463.
68 M. Brinkmann, L. Hartmann, L. Biniek, K. Tremel, N. Kayunkid, *Macromol. Rapid Commun.* **2014**, *35*, 9.
69 N. Kayunkid, S. Uttiya, M. Brinkmann, *Macromolecules* **2010**, *43*, 4961.
70 T. Breuer, M. Klues, G. Witte, *J. Electron Spectrosc. Relat. Phenom.* **2015**, *204*, 102.
71 S. S. Dalal, D. M. Walters, I. Lyubimov, J. J. de Pablo, Ediger, *Proc. Natl. Acad. Sci. U.S.A.* **2015**, *112*, 4227.
72 B. S. Bhardwaj, T. Sugiyama, N. Namba, T. Umakoshi, T. Uemura, T. Sekitani, P. Verma, *Sci. Rep.* **2019**, *9*, 15149.
73 S. Wood, G.-P. Rigas, A. Zoladek-Lemanczyk, J. C. Blakesley, S. Georgakopoulos, M. Mas-Torrent, M. Shkunov, F. A. Castro, *Sci. Rep.* **2016**, *6*, 33057.
74 T. Mino, Y. Saito, H. Yoshida, S. Kawata, P. Verma, *J. Raman Spectrosc.* **2012**, *43*, 2029.
75 Y. Furukawa, K. Seto, K. Nakajima, Y. Itoh, J. Eguchi, T. Sugiyama, H. Fujimura, *Vib. Spectrosc.* **2012**, *60*, 5.
76 D. Bhattacharyya, A. Montenegro, P. Dhar, M. Mammetkuliyev, R. M. Pankow, M. C. Jung, M. E. Thompson, B. C. Thompson, A. V. Benderskii, *J. Phys. Chem. Lett.* **2019**, *10*, 1757.
77 M. Xiao, J. Jasensky, X. Zhang, Y. Li, C. Pichan, X. Lu, Z. Chen, *Phys. Chem. Chem. Phys.* **2016**, *18*, 22089.
78 F. C. B. Maia, P. B. Miranda, *J. Phys. Chem. C* **2015**, *119*, 7386.
79 M. Xiao, X. Zhang, Z. J. Bryan, J. Jasensky, A. J. McNeil, Z. Chen, *Langmuir* **2015**, *31*, 5050.
80 A. Sugie, W. Han, N. Shioya, T. Hasegawa, H. Yoshida, *J. Phys. Chem. C* **2020**, *124*, 9765.
81 N. Shioya, R. Fujiwara, K. Tomita, T. Shimoaka, T. Hasegawa, *J. Phys. Chem. A* **2020**, *124*, 2714.
82 T. Nakamura, N. Shioya, T. Hasegawa, Y. Murata, R. Murdey, A. Wakamiya, *ChemPlusChem* **2019**, *84*, 1396.
83 K. Tomita, N. Shioya, T. Shimoaka, K. Eda, T. Hasegawa, *Bull. Chem. Soc. Jpn.* **2019**, *92*, 1335.
84 M. A. Truong, J. Lee, T. Nakamura, J.-Y. Seo, M. Jung, M. Ozaki, A. Shimazaki, N. Shioya, T. Hasegawa, Y. Murata, S. M. Zakeeruddin, M. Grätzel, R. Murdey, A. Wakamiya, *Chem.—Eur. J.* **2019**, *25*, 6741.
85 T. Nakamura, N. Shioya, T. Shimoaka, R. Nishikubo, T. Hasegawa, A. Saeki, Y. Murata, R. Murdey, A. Wakamiya, *Chem. Mater.* **2019**, *31*, 1729.
86 N. Shioya, R. Murdey, K. Nakao, H. Yoshida, T. Koganezawa, K. Eda, T. Shimoaka, T. Hasegawa, *Sci. Rep.* **2019**, *9*, 579.
87 K. Tomita, N. Shioya, R. Kise, T. Shimoaka, H. Yoshida, T. Koganezawa, K. Eda, T. Hasegawa, *Thin Solid Films* **2018**, *665*, 85.
88 N. Shioya, M. Hada, T. Shimoaka, R. Murdey, K. Eda, T. Hasegawa, *J. Phys. Chem. C* **2018**, *122*, 4540.
89 K. Abiko, Y. Kato, *Chem. Lett.* **2018**, *47*, 332.
90 N. Shioya, T. Shimoaka, K. Eda, T. Hasegawa, *Macromolecules* **2017**, *50*, 5090.
91 M. Hada, N. Shioya, T. Shimoaka, K. Eda, M. Hada, T. Hasegawa, *Chem.—Eur. J.* **2016**, *22*, 16539.
92 N. Shioya, T. Shimoaka, K. Eda, T. Hasegawa, *Phys. Chem. Chem. Phys.* **2015**, *17*, 13472.
93 A. Wadsworth, Z. Hamid, M. Bidwell, R. S. Ashraf, J. I. Khan, D. H. Anjum, C. Cendra, J. Yan, E. Rezasoltani, A. A. Y. Guilbert, M. Azzouzi, N. Gasparini, J. H. Bannock, D. Baran, H. Wu, J. C. de Mello, C. J. Brabec, A. Salleo, J. Nelson, F. Laquai, I. McCulloch, *Adv. Energy Mater.* **2018**, *8*, 1801001.
94 S. Agbolaghi, S. Zenoozi, *Org. Electron.* **2017**, *51*, 362.
95 M. Brinkmann, *J. Polym. Sci., Part B: Polym. Phys.* **2011**, *49*, 1218.
96 A. Gujral, J. Gómez, J. Jiang, C. Huang, K. A. O'Hara, M. F. Toney, M. L. Chabinyc, L. Yu, M. D. Ediger, *Chem. Mater.* **2017**, *29*, 849.
97 G. Louarn, M. Trznadel, J. P. Buisson, J. Laska, A. Pron, M. Lapkowski, S. Lefrant, *J. Phys. Chem.* **1996**, *100*, 12532.
98 S. Obata, Y. Shimoi, *Phys. Chem. Chem. Phys.* **2013**, *15*, 9265.
99 J. Kesters, P. Verstappen, M. Kelchtermans, L. Lutsen, D. Vanderzande, W. Maes, *Adv. Energy Mater.* **2015**, *5*, 1500218.
100 M. G. Walter, A. B. Rudine, C. C. Wamser, *J. Porphyr. Phthalocyanines* **2010**, *14*, 759.
101 S. Ishihara, J. Labuta, W. V. Rossom, D. Ishikawa, K. Minami, J. P. Hill, K. Ariga, *Phys. Chem. Chem. Phys.* **2014**, *16*, 9713.
102 J. Spadavecchia, G. Ciccarella, P. Siciliano, S. Capone, R. Rella, *Sens. Actuators, B* **2004**, *100*, 88.
103 X.-B. Zhang, C.-C. Guo, Z.-Z. Li, G.-L. Shen, R.-Q. Yu, *Anal. Chem.* **2002**, *74*, 821.
104 A. Afzali, C. D. Dimitrakopoulos, T. L. Breen, *J. Am. Chem. Soc.* **2002**, *124*, 8812.
105 Y. Hosoi, K. Okamura, Y. Kimura, H. Ishii, M. Niwano, *Appl. Surf. Sci.* **2005**, *244*, 607.
106 T. Hasegawa, Y. Itoh, A. Kasuya, *Anal. Chem.* **2008**, *80*, 5630.
107 A. Kasuya, Y. Itoh, T. Okada, M. Osawa, Y. Takahashi, E. Kazuma, T. Tatsuma, T. Hasegawa, *Phys. Chem. Chem. Phys.* **2011**, *13*, 9691.
108 R. Ruiz, D. Choudhary, B. Nickel, T. Toccoli, K.-C. Chang, A. C. Mayer, P. Clancy, J. M. Blakely, R. L. Headrick, S. Iannotta, G. G. Malliaras, *Chem. Mater.* **2004**, *16*, 4497.
109 J. E. Northrup, M. L. Tiago, S. G. Louie, *Phys. Rev. B: Condens. Matter Mater. Phys.* **2002**, *66*, 121404.
110 Y. Zeng, B. Tao, Z. Yin, *J. Cryst. Growth* **2014**, *405*, 73.
111 M.-C. Jung, M. R. Leyden, G. O. Nikiforov, M. V. Lee, H.-K. Lee, T. J. Shin, K. Takimiya, Y. Qi, *ACS Appl. Mater. Interfaces* **2015**, *7*, 1833.
112 A. C. Dürr, B. Nickel, V. Sharma, U. Täffner, H. Dosch, *Thin Solid Films* **2006**, *503*, 127.
113 A. Kubono, R. Akiyama, *Mol. Cryst. Liq. Cryst.* **2002**, *378*, 167.
114 C. D. Dimitrakopoulos, A. R. Brown, A. Pomp, *J. Appl. Phys.* **1996**, *80*, 2501.
115 T. Minakata, H. Imai, M. Ozaki, *J. Appl. Phys.* **1992**, *72*, 4178.
116 K. O. Lee, T. T. Gan, *Chem. Phys. Lett.* **1977**, *51*, 120.
117 Y. Kamura, I. Shirotani, H. Inokuchi, Y. Maruyama, *Chem. Lett.* **1974**, *3*, 627.
118 N. Shioya, K. Tomita, T. Shimoaka, T. Hasegawa, *J. Phys. Chem. A* **2019**, *123*, 7177.
119 T. Hasegawa, T. Shimoaka, N. Shioya, K. Morita, M. Sonoyama, T. Takagi, T. Kanamori, *ChemPlusChem* **2014**, *79*, 1421.
120 T. Hasegawa, *Chem. Rec.* **2017**, *17*, 903.
121 T. Shimoaka, M. Sonoyama, H. Amii, T. Takagi, T. Kanamori, T. Hasegawa, *J. Phys. Chem. A* **2019**, *123*, 3985.

122 R. Kise, A. Fukumi, N. Shioya, T. Shimoaka, M. Sonoyama, H. Amii, T. Takagi, T. Kanamori, K. Eda, T. Hasegawa, *Bull. Chem. Soc. Jpn.* **2019**, *92*, 785.
123 C. Wang, S. K. Sharma, O. S. Olaluwoye, S. A. Alrashdi, T. Hasegawa, R. M. Leblanc, *Colloids Surf., B* **2019**, *183*, 110401.
124 C. Wang, T. Hosomi, K. Nagashima, T. Takahashi, G. Zhang, M. Kanai, H. Zeng, W. Mizukami, N. Shioya, T. Shimoaka, T. Tamaoka, H. Yoshida, S. Takeda, T. Yasui, Y. Baba, Y. Aoki, J. Terao, T. Hasegawa, T. Yanagida, *Nano Lett.* **2019**, *19*, 2443.
125 K. Sakakibara, K. Nishiumi, T. Shimoaka, T. Hasegawa, Y. Tsujii, *Macromolecules* **2019**, *52*, 6673.
126 R. Imanishi, Y. Nagashima, M. Hara, S. Nagano, T. Seki, *Chem. Lett.* **2019**, *48*, 98.
127 Y. Nagao, *Langmuir* **2017**, *33*, 12547.
128 R. Ishige, K. Tanaka, S. Ando, *Macromol. Chem. Phys.* **2018**, *219*, 1700370.